CrossMark

NEURO

Dual-energy CT of the brain: Comparison between DECT angiography-derived virtual unenhanced images and true unenhanced images in the detection of intracranial haemorrhage

Matteo Bonatti[1] · Fabio Lombardo[2] · Giulia A. Zamboni[2] · Patrizia Pernter[1] ·
Roberto Pozzi Mucelli[2] · Giampietro Bonatti[1]

Abstract

Objective To evaluate the diagnostic performance of virtual non-contrast (VNC) images in detecting intracranial haemorrhages (ICHs).

Methods Sixty-seven consecutive patients with and 67 without ICH who underwent unenhanced brain CT and DECT angiography were included. Two radiologists independently evaluated VNC and true non-contrast (TNC) images for ICH presence and type. Inter-observer agreement for VNC and TNC image evaluation was calculated. Sensitivity and specificity of VNC images for ICH detection were calculated using Fisher's exact test. VNC and TNC images were compared for ICH extent (qualitatively and quantitatively) and conspicuity assessment.

Results On TNC images 116 different haemorrhages were detected in 67 patients. Inter-observer agreement ranged from 0.98–1.00 for TNC images and from 0.86–1.00 for VNC images. VNC sensitivity ranged from 0.90–1, according to the different ICH types, and specificity from 0.97–1. Qualitatively, ICH extent was underestimated on VNC images in 11.9% of cases. Haemorrhage volume did not show statistically significant differences between VNC and TNC images. Mean haemorrhage conspicuity was significantly lower on VNC images than on TNC images for both readers ($p < 0.001$).

Conclusion VNC images are accurate for ICH detection. Haemorrhages are less conspicuous on VNC images and their extent may be underestimated.

Key points
- *VNC images represent a reproducible tool for detecting ICH.*
- *ICH can be identified on VNC images with high sensitivity and specificity.*
- *Intracranial haemorrhages are less conspicuous on VNC images than on TNC images.*
- *Intracranial haemorrhages extent may be underestimated on VNC images.*

Keywords Multidetector computed tomography ·
Dual-energy, Virtual non-contrast · Intracranial haemorrhage ·
Brain · Emergencies

Abbreviations and acronyms

CT	Computed tomography
CTA	Computed tomography angiography
DECT	Dual-energy CT
ICH	Intracranial haemorrhage
ROI	Region of interest
TNC	True non-contrast
VNC	Virtual non-contrast

✉ Matteo Bonatti
matteobonatti@hotmail.com

[1] Department of Radiology, Bolzano Central Hospital, 5 Boehler Street, 39100 Bolzano, Italy

[2] Department of Radiology, University of Verona, 10 LA Scuro Place, 37134 Verona, Italy

Introduction

The incidence of intracranial haemorrhage (ICH) ranges between 10 and 20 cases per 100,000 inhabitants per year and increases with age. Hypertension and amyloid angiopathy represent the most common causes of non-traumatic intracranial bleedings, followed by vascular abnormalities (i.e. intracranial aneurysms, cavernous

angiomas and artero-venous malformations), coagulopathies and tumours [1]. According to the involved anatomical site, ICHs can be subdivided into epidural, subdural, subarachnoid, intraparenchymal and intraventricular.

Thanks to its wide availability, cost-effectiveness and high accuracy in differentiating blood from brain tissue, cerebrospinal fluid and bone, nowadays unenhanced computed tomography (CT) represents the imaging modality of choice for ICH identification and characterization; moreover, brain CT angiography (CTA) is indicated in patients affected by ICH with possible vascular origin [2, 3]. If technically available, a dual-energy technique should be used for CTA acquisition [4]. Indeed, dual-energy CT (DECT), thanks to its three-material decomposition capability [5, 6], warrants higher quality reconstructions than single-energy CT, without any significant increase in radiation dose [7, 8]. In addition, low-keV monoenergetic reconstructions may be obtained from DECT datasets, which may further improve CTA quality as vessel attenuation significantly increases at lower energies [9]. Three-material decomposition algorithms may also be used for subtracting iodine density present in each voxel, obtaining virtual non-contrast (VNC) reconstructions from post-contrast images. VNC reconstructions are currently used for differentiating bleeding from contrast material extravasation secondary to blood-brain barrier damage in patients who underwent mechanical thrombectomy [10–16].

Only a few studies in the literature considered the possibility of using virtual unenhanced images derived from CTA acquisitions for ICH detection, with encouraging results [15, 16]. The aim of our study was to evaluate the diagnostic performance of VNC reconstructions generated from DECT-angiography images in the detection and characterization of ICH.

Materials and methods

Patient population

This was a retrospective study approved by our Institutional Review Board; need for informed consent was waived. We considered for inclusion in our study 12,288 consecutive patients who underwent unenhanced brain CT at our Institution in the period July 2013–July 2015 after admission to the Emergency Department. Two different groups of patients were included in our study.

For the first group, inclusion criteria were presence of ICH at unenhanced CT (501/12,288 patients) and subsequent performance of brain DECT-angiography within 1 h to clarify the origin of the bleeding, e.g. to demonstrate presence of intracranial aneurysms or vascular malformations (72/501 patients). The sole exclusion criterion was insufficient image quality because of motion artefacts (5/72 patients). Therefore, the first group comprised 67 patients.

For the second group, inclusion criteria were absence of ICH at unenhanced CT (11,787/12,288 patients) and subsequent performance of brain DECT-angiography, within 1 h, on suspicion of intracranial artery occlusion (95/11,787 patients). Again, the sole exclusion criterion was insufficient image quality because of motion artefacts (4/95 patients). We randomly selected 67 patients from this group of 91, in order to have exactly the same number of negative controls.

Therefore, our study population included 134 patients, 76 females and 58 males, with a median age of 64 years (range 18–93 years): 67 with and 67 without ICH.

Imaging protocol

All the examinations were performed on a second-generation dual-source CT scanner (Somatom Definition Flash; Siemens Healthcare, Forchheim, Germany) equipped with a tin filter, with the patient lying supine on the table with arms down the side of the body. Scanning parameters are given in Table 1. Unenhanced brain CT images were obtained using a single-energy spiral technique at 120 kV, and brain CTA images were obtained with dual-energy acquisition (80 kVp for low-energy tube, Sn140 kVp for high-energy tube). DECT-angiograms were obtained after intravenous administration of 75 ml of 350 mg iodine/ml iodinated contrast material (Iobitridol, Xenetix 350, Guerbet, France), at a flow rate of 4 ml/s, followed by a 50-ml of saline flush, through an 18-gauge catheter placed in an antecubital vein using an automatic power injector (Stellant Medrad, Indianola, PA, USA); a bolus-tracking technique was adopted, with the region of interest (ROI) placed in the common carotid artery at the level of C4 (threshold 100 Hounsfield units (HU), scan delay 4 s).

Table 1 Scanning parameters for unenhanced brain CT and dual-energy CT (DECT) brain angiography

	Unenhanced brain CT	DECT brain angiography
Scanning technique	Spiral	Spiral
Scan direction	Caudo-cranial	Caudo-cranial
kVp	120	80/Sn140
mAs ref	390	222/111
Collimation	128x0.6 mm	64x0.6 mm
Rotation time	1.0 s	0.33 s
Pitch	0.55	0.7
Care-DOSE 4D	On	Off
Care-kV	Off	Not available
X-care	On	Not available
Kernel	H40s medium	D26f med. smooth ASA

Image analysis

VNC images were generated from the DECT-angiography datasets using commercially available software (Syngo.Via Brain Haemorrhage Application, Version VA30A, Siemens, Erlangen, Germany) on a workstation. Software parameters were set according to manufacturer recommendations: resolution = 1, maximum = 3,071 HU and iodine ratio = 3.01.

Two radiologists, reader 1 and reader 2, with 7 and 4 years of experience in diagnostic neuroradiology, respectively, blinded to patients' clinical data, independently evaluated the VNC images of each patient (positive cases and negative controls, randomly) using 5-mm thick multiplanar reconstructions on axial, coronal and sagittal planes. Window levels were set according to the vendor's recommendation (L = 40, W = 100) and manually adjusted as needed. Each reader was asked to assess the presence of intracranial bleeding (present/absent) and to note its specific location as epidural (present/absent), subdural (present/absent), subarachnoid (present/absent), intraparenchymal (present/absent) or intraventricular (present/absent). Furthermore, each reader was called to subjectively express his diagnostic confidence using a 5-point scale (1 = non-diagnostic, 2 = poor, 3 = moderate, 4 = good, 5 = excellent). Subsequently, the two readers independently evaluated the TNC images of all patients (positive cases and negative controls, randomly), using the same parameters as for VNC ones. Each reader was asked to assess the presence of intracranial bleeding (present/absent) and to note its specific location as epidural (present/absent), subdural (present/absent), subarachnoid (present/absent), intraparenchymal (present/absent) or intraventricular (present/absent); discrepancies were then solved by consensus. Also for TNC images diagnostic confidence was stated using a 5-point scale (1 = non-diagnostic, 2 = poor, 3 = moderate, 4 = good, 5 = excellent). TNC images were considered the reference standard for this study.

After that, for positive cases the two readers independently measured haemorrhage attenuation and normal brain tissue attenuation in the contralateral hemisphere on both datasets using round ROIs. Haemorrhages with the shortest axis <3 mm were excluded from this evaluation in order to minimize partial volume artefacts. Haemorrhage conspicuity was calculated as the difference in attenuation between blood and healthy brain tissue.

Furthermore, the two image datasets (TNC and VNC) of each patient with ICH on TNC images (67/114) were evaluated side-by-side by the two radiologists in consensus using the same field of view (FoV), slice thickness and inclination. Haemorrhage extent was qualitatively compared on the two datasets (larger on TNC, larger on VNC, or similar on TNC and VNC).

Finally, the volume of intraparenchymal, intraventricular and subdural haemorrhages with the shortest axis >3 mm

was calculated by the two readers in consensus on TNC and VNC images using an open-source DICOM viewer software for MAC (OsiriX Imaging Software, Version 7.5.1, www. osirix-viewer.com). Freehand ROIs were manually mapped around the haemorrhage on continuous CT slices and the software automatically calculated haemorrhage volume.

Dose reports for each patient were reviewed; Computed Tomography Dose Index for the volume (CTDIvol) and Dose Length Product (DLP) were annotated for each acquisition. Effective dose (ED) for each acquisition was estimated according to the formula: ED = DLP * 0.0021 [17].

Statistical analysis

Inter-observer agreement in VNC and TNC images evaluation was calculated according to the weighted kappa-statistics using GraphPad QuickCalcs, www.graphpad.com. Agreement was assessed as follows: very good if k = 0.81–1.00, good if k = 0.61–0.80, moderate if k = 0.41–0.60, fair if k = 0.21–0.40, poor if k < 0.20).

Sensitivity, specificity, positive predictive value and negative predictive value of VNC images for the detection of each different haemorrhage subtype were calculated for each reader.

Fisher's exact test and the paired t-test were performed using GraphPad Prism version 6.00 for Mac OS X (GraphPad Software, La Jolla, CA, USA, www.graphpad.com).

Results

Qualitative imaging evaluation

On TNC images, both readers identified 67 patients affected by ICH. Reader 1 found 47 subarachnoid haemorrhages, 33 intraparenchymal haemorrhages, 21 intraventricular haemorrhages, 14 subdural haemorrhages and no epidural haemorrhages, whereas reader 2 found 48 subarachnoid haemorrhages, 33 intraparenchymal haemorrhages, 21 intraventricular haemorrhages, 14 subdural haemorrhages and no epidural haemorrhages. Interobserver agreement for TNC image evaluation was 0.984 (95% confidence interval (CI) 0.952–1.000) for subarachnoid haemorrhage, 1.000 (95% CI 1.000–1.000) for intraparenchymal haemorrhage, 1.000 (95% CI 1.000–1.000) for intraventricular haemorrhage and 1.000 (95% CI 1.000–1.000) for subdural haemorrhage. After consensus, 48 patients were classified as having subarachnoid haemorrhage, 33 patients as having intraparenchymal haemorrhage, 21 patients as having intraventricular haemorrhage, 14 patients as having subdural haemorrhage, and no patients as having epidural haemorrhage. Therefore, 116 different haemorrhages were detected in 67 patients: 30 patients

showed one type of haemorrhage, 24 patients two types and 13 patients three types. Mean diagnostic confidence in ICH detection on TNC images was 4.8/5 for reader 1 (median 5/5) and 4.9/5 for reader 2 (median 5/5).

On VNC images, reader 1 identified 66 patients affected by ICH, whereas reader 2 identified 68 patients affected by ICH. Reader 1 detected 14 subdural haemorrhages, 48 subarachnoid haemorrhages, 31 intraparenchymal haemorrhages and 20 intraventricular haemorrhages; among these there were one false-positive and one false-negative case of subdural haemorrhage, three false-positive and three false-negative cases of subarachnoid haemorrhage, two false-negative cases of intraparenchymal haemorrhage and one false-positive and two false-negative cases of intraventricular haemorrhage (Figs. 1 and 2). Reader 2 detected 15 subdural haemorrhages, 44 subarachnoid haemorrhages, 35 intraparenchymal haemorrhages and 21 intraventricular haemorrhages; among these, there were one false-positive case of subdural haemorrhage, four false-negative cases of subarachnoid haemorrhage,
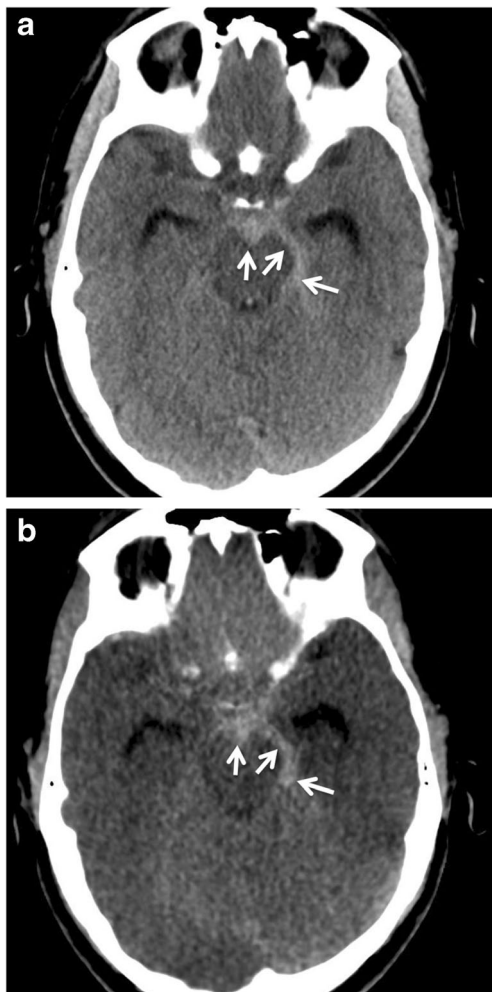

Fig. 1 Five-mm thick axial true non-contrast (**a**) and virtual non-contrast (**b**) images (window levels: L = 40 HU, W = 100 HU) show a similar extent for this subarachnoid haemorrhage (arrows.
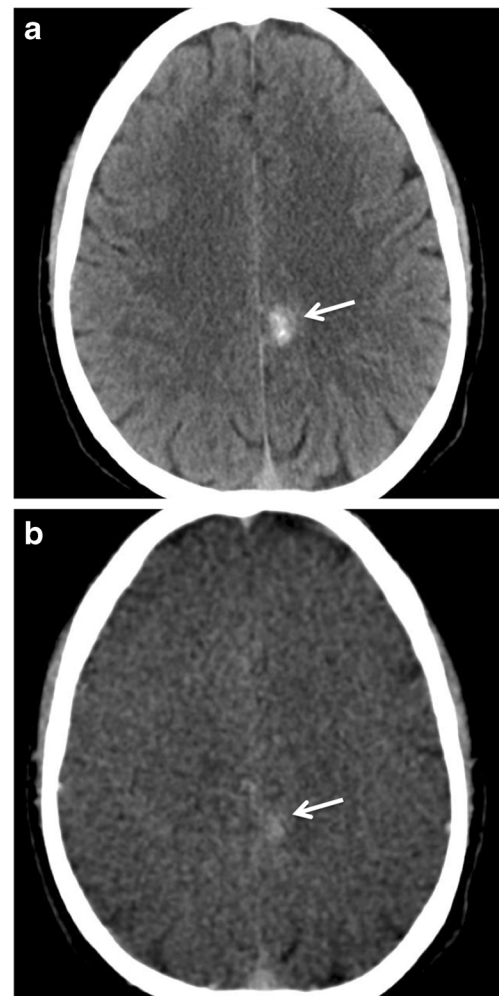

Fig. 2 Haemorrhage extent underestimation. The extent of this intraparenchymal haemorrhage (arrow) was underestimated on 5-mm thick axial virtual non-contrast (VNC) images (**b**) in comparison with 5-mm thick axial true non-contrast images (**a**) (window levels: L = 40 HU, W = 100 HU). Both readers correctly detected this haemorrhage on VNC images. The patient showed signs of amyloid angiopathy on a subsequent MRI

three false-positive and one false-negative cases of intraparenchymal haemorrhage, and two false-positive and two false-negative cases of intraventricular haemorrhage (Figs. 1 and 2). Both readers missed three subarachnoid haemorrhages, one intraparenchymal haemorrhage and one intraventricular haemorrhage in the same patients. Inter-observer agreement for VNC image evaluation was 0.961 (95% CI 0.886–1.000) for subdural haemorrhage, 0.934 (95% CI 0.870–0.998) for subarachnoid haemorrhage, 0.920 (95% CI 0.842–0.997) for intraparenchymal haemorrhage and 0.856 (95% CI 0.733–0.979) for intraventricular haemorrhage. Accuracy, sensitivity, specificity, positive predictive value and negative predictive value of VNC images for the detection of each specific type of haemorrhage for each reader are reported in Table 2. Mean diagnostic confidence in ICH

Table 2 Diagnostic performance of virtual non-contrast images for the detection of each specific intracranial haemorrhage subtype for each reader

	Accuracy		Sensitivity		Specificity		PPV		NPV	
	R1	R2	R1	R2	R1	R2	R1	R2	R1	R2
Subdural	132/134 (0.99)	133/134 (0.99)	13/14 (0.93)	14/14 (1.00)	119/120 (0.99)	119/120 (0.99)	13/14 (0.93)	14/15 (0.93)	119/120 (0.99)	119/119 (1.00)
Subarachnoid	128/134 (0.96)	130/134 (0.97)	45/48 (0.94)	44/48 (0.92)	83/86 (0.97)	86/86 (1.00)	45/48 (0.94)	44/44 (1.00)	83/86 (0.97)	86/90 (0.96)
Intraparenchymal	132/134 (0.99)	130/134 (0.97)	31/33 (0.94)	32/33 (0.97)	101/101 (1.00)	98/101 (0.97)	31/31 (1.00)	32/35 (0.91)	101/103 (0.98)	98/99 (0.99)
Intraventricular	131/134 (0.98)	130/134 (0.97)	19/21 (0.90)	19/21 (0.90)	112/113 (0.99)	111/113 (0.98)	19/20 (0.95)	19/21 (0.90)	112/114 (0.98)	111/113 (0.98)

PPV positive predictive value, *NPV* negative predictive value, *R1* reader 1, *R2* reader 2

detection on VNC images was 4.1/5 for reader 1 (median 4/5) and 4.3/5 for reader 2 (median 4/5).

By comparing TNC and VNC images of each patient side by side, haemorrhage extent was similar on both series in 59/67 (88.1%) cases (Fig. 3), whereas it was underestimated on VNC images in the remaining 8/67 (11.9%) cases (Fig. 4).

Quantitative imaging evaluation

One hundred and one of 116 haemorrhages were included in the quantitative imaging evaluation: 35/47 subarachnoid haemorrhages, 32/33 intraparenchymal haemorrhages, 21/21 intraventricular haemorrhages and 13/14 subdural haemorrhages.

Mean haemorrhage attenuation was 61 ± 10 HU on TNC images and 59 ± 10 HU on VNC images for
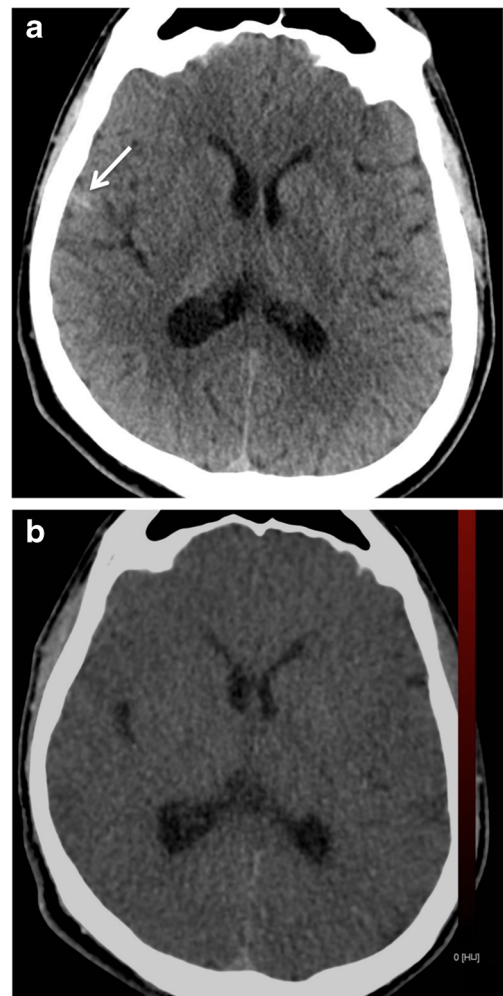

Fig. 3 A false-negative case. On 5-mm thick axial true non-contrast images (**a**) a small subarachnoid haemorrhage (arrow) is recognizable in a cortical sulcus of the right temporal lobe. This haemorrhage was not visible on virtual non-contrast images, and neither radiologist detected it (**b**) (window levels: L = 40 HU, W = 100 HU)
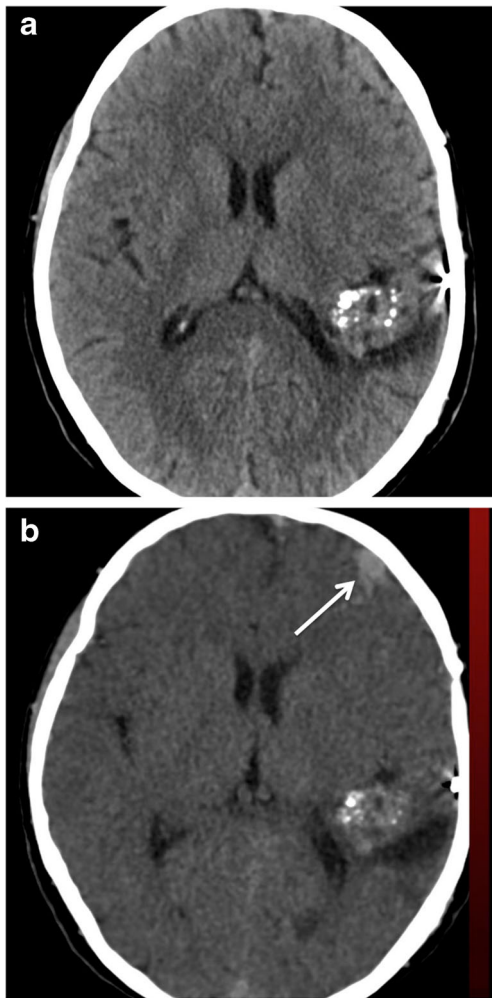
Fig. 4 A false-positive case. On true non-contrast images (**a**) no intra-cranial haemorrhage is present in this patient who previously underwent artero-venous malformation embolization. A small subarachnoid haemorrhage (arrow) was suspected by one of the two readers on virtual non-contrast images (**b**). This false-positive result was due to incomplete iodine subtraction within pathologically enlarged vessels

VNC images for reader 2. Mean haemorrhage conspicuity was 31 ± 9 HU on TNC images and 24 ± 10 HU on VNC images for reader 1, and 29 ± 10 on TNC images and 23 ± 9 on VNC images for reader 2. Mean brain tissue attenuation was significantly lower on TNC images than on VNC ones for both readers (paired t-test, $p < 0.001$ for both readers), whereas no significant difference was found in blood attenuation ($p > 0.05$ for both readers). Haemorrhage conspicuity was significantly lower on VNC images than on TNC images for both readers ($p < 0.001$ for both readers).

Haemorrhage volume on TNC and VNC images was calculated for 66 haemorrhages: 32/33 intraparenchymal haemorrhages, 21/21 intraventricular haemorrhages and 13/14 subdural haemorrhages. Mean haemorrhage volume was 22.09 ± 19.26 cc on TNC images and 21.96 ± 19.86 cc on VNC images ($p > 0.05$). Mean haemorrhage volume difference between TNC and VNC images was 0.1 ± 3.8 cc ($p > 0.05$); haemorrhage volume on TNC images was, on average, $5 \pm 22\%$ larger than on VNC ones ($p > 0.05$).

Data on CTDIvol, DLP and ED of single-energy unenhanced brain CT and dual-energy brain CTA are reported in Table 3.

Discussion

Our study confirmed that unenhanced brain CT represents an extremely reproducible tool for identifying and characterizing ICHs, but also that VNC images warrant an excellent performance for this aim. Indeed, in our series, interobserver agreement was classified as 'very good' for all the evaluated parameters, on both TNC and VNC images, with k-values ranging from 0.98 (presence of subarachnoid haemorrhage) to 1.00 (all the other parameters) for TNC images and from 0.86 (presence of intraventricular haemorrhage) to 0.96 (presence of subdural haemorrhage) for VNC images. Both readers felt very confident in ICH detection on VNC images, with mean subjective confidence values of 4.1/5 for reader 1 and of 4.3/5, for reader 2; confidence values were significantly lower than for TNC images (4.8/5 for reader 1 and 4.9/5 for reader 2) ($p < 0.001$).

reader 1, and 60 ± 9 HU on TNC images and 58 ± 10 HU on VNC images for reader 2. Mean healthy contralateral brain tissue attenuation was 30 ± 5 HU on TNC images and 35 ± 5 HU on VNC images for reader 1, and 31 ± 6 HU on TNC images and 35 ± 6 HU on

Table 3 Data on Computed Tomography Dose Index for the volume (CTDIvol), Dose Length Product (DLP) and Effective Dose (ED) of single-energy unenhanced brain CT and dual-energy brain CT angiography

	Mean CTDIvol (mGy)	Mean DLP (mGycm)	ED (mSv)
Single-energy unenhanced brain CT	54.99 ± 3.68 (range 48.09–69.77)	961 ± 92 (range 794–1361)	2.02 ± 0.19 (range 1.67–2.86)
Dual-energy brain CT angiography	19.30 ± 0.02 (range 19.6–19.35)	372 ± 37 mGycm (range 257–627 mGycm)	0.78 ± 0.08 (range 0.54–1.32)

VNC images appeared to be accurate in the detection of the different ICH types, with sensitivity ranging from 0.90 to 1 and specificity from 0.97 to 1 according to the different haemorrhage types, and accuracy values ranging from 0.96 to 0.99. In particular VNC appeared to be extremely useful for excluding the presence of ICH, with negative predictive values ranging from 0.96 to 1 according to the different haemorrhage types. Anyway, a non-negligible number of false-negative cases were observed in our series: 8/116 (6.9%) for reader 1 and 7/116 (6.0%) for reader 2. Among these, we found five cases (three subarachnoid haemorrhages, one intraparenchymal haemorrhage and one intraventricular haemorrhage) in which both readers independently did not recognize the same haemorrhage on VNC images. A later review of these cases with a direct side-by-side comparison of VNC and TNC images, made by the two readers in consensus, highlighted that the lower tissue contrast resolution of VNC images in comparison with TNC ones (Fig. 3a, b) associated with their lower intrinsic contrast-to-noise ratio were the causes of these evaluation errors. Moreover, some false-positive cases were also observed in our series: 5/116 (4.3%) for reader 1 and 6/116 (5.2%) for reader 2. False-positive cases were mainly the consequence of incomplete iodine subtraction (Fig. 4a, b): although quite unlikely, the onset of a new bleed in the time elapsed between the TNC scan and the CTA acquisition cannot be excluded with certainty. Furthermore, in these cases the lower signal-to-noise ratio of VNC images in comparison to TNC ones played a relevant role.

The quantitative evaluation of haemorrhage conspicuity demonstrated that bleedings are significantly less conspicuous on VNC images than on TNC images, mainly as a consequence of the relatively higher attenuation of normal brain tissue on VNC images in comparison with TNC images, which leads to a reduced difference in attenuation between blood and brain tissue. Even if attenuation values measured on VNC images are considered reliable and similar to the ones measured on TNC images, differences in the order of 10–15 HU have already been described in the literature [18–20]. This evidence is substantially confirmed by our study in which the differences in absolute attenuation values were relatively small; furthermore, in the central nervous system small differences also play a relevant role given the physiologically small attenuation differences between different anatomical structures. The reason for these discrepancies is not completely clear and probably multifactorial. A possible explanation might reside in beam-hardening artefacts [21, 22] generated by the contrast-filled arteries on CTA that in our series could have been enhanced by the low-dose protocol adopted for CTA. Another cause may reside in VNC reconstruction software parameter settings. We performed VNC reconstruction using manufacturer-suggested parameters, but some trimming in software settings might increase iodine subtraction accuracy [23].

The qualitative comparison of VNC and TNC images revealed that haemorrhage extent was underestimated on VNC in 11.9% of the cases. This result is partially also supported by quantitative image analysis results that, although not reaching statistical significance and having been performed on 66/116 haemorrhages only, showed that haemorrhage volume was larger on TNC images than on VNC ones in the majority of the cases, with a mean difference of +5% on TNC images. These findings suggest that patients with small haemorrhages might remain undiagnosed on VNC images and raise the suspicion that the use of the VNC images as the only basis for ICH detection may not be safe enough to be routinely adopted in clinical practice.

By evaluating our results, it must be taken into account that, according to our scanning protocol, DECT angiography is performed using significantly lower x-ray intensity than single-energy unenhanced brain CT (mAs ref 222/111 vs. 390). This setting warrants a significant reduction in radiation dose (mean estimated ED was 0.78 mSv for CTA and 2.02 mSv for unenhanced brain CT), but it also contributes to reducing image quality of VNC reconstructions, which may lead to a reduction in accuracy in ICH characterization.

To our knowledge, there are already two published studies that suggested the possibility of using VNC images derived from DECT-angiography for the detection of ICH. The study by Ferda et al. concluded that VNC images are able to reveal the presence of ICHs with high accuracy; however, the study population was relatively small (25 patients) and included only patients with known ICH [15]. On the other hand, the study by Jiang et al. included 84 patients and stated that VNC images are a reliable tool for detecting subarachnoid haemorrhages, even acknowledging the possibility of false-negative results [16]. These limitations were partially overcome in our study, which included a greater number of patients with proven ICH and a group of negative controls. However, our study does have some limitations, the most important of which resides in its retrospective design. Secondly, the same radiologists reviewed both VNC and TNC images, which may represent a study bias, even if blinded to patients' clinical data. Further studies performing DECT angiography using higher x-ray intensities or different reconstruction algorithms (e.g. iterative reconstruction) are needed in order to better assess VNC image performance in the detection of small ICHs.

In conclusion, our study confirmed the reliability of VNC images in detecting and characterizing ICHs, but it also demonstrated that small haemorrhages might be missed on VNC images due to their lower conspicuity. Unenhanced brain CT remains the gold standard for the initial evaluation of patients with acute neurological symptoms and should always be performed as a first-line examination in these cases. VNC images can be considered adequate tfor diagnostic purposes when performing brain DECT-angiography in patients with known

brain haemorrhage (e.g. in case of subsequent controls). Moreover, unenhanced brain CT is often performed in patients undergoing brain-CTA in a non-emergency setting (e.g. for aneurisms clipping follow-up or after AVM embolization); in our opinion, this stage could be skipped using DECT-derived VNC reconstructions.

References

1. Qureshi AI, Tuhrim S, Broderick JP, Batjer HH, Hondo H, Hanley DF (2001) Spontaneous intracerebral hemorrhage. NEJM 344: 1450–1460

2. Lu L, Zhang LJ, Poon CS et al (2012) Digital subtraction CT angiography for detection of intracranial aneurysms: comparison with three-dimensional digital subtraction angiography. Radiology 262: 605–612

3. Westerlaan HE, van Dijk JM, Jansen-van der Weide MC et al (2011) Intracranial aneurysms in patients with subarachnoid hemorrhage: CT angiography as a primary examination tool for diagnosis: systematic review and meta-analysis. Radiology 258:134–145

4. Zhang LJ, Wu SY, Poon CS et al (2010) Automatic bone removal dual-energy CT angiography for the evaluation of intracranial aneurysms. J Comput Assist Tomogr 34:816–824

5. Johnson TR, Krauss B, Sedlmair M et al (2007) Material differentiation by dual energy CT: initial experience. Eur Radiol 17:1510–1517

6. McCollough CH, Leng S, Yu L, Fletcher JG (2015) Dual- and multi-energy CT: principles, technical approaches, and clinical applications. Radiology 276:637–653

7. Hegde A, Chan LL, Tan L, Illyyas M, Lim WE (2009) Dual Energy CT and its use in neuroangiography. Ann Acad Med Singap 38: 817–820

8. Postma AA, Hofman PA, Stadler AA, van Oostenbrugge RJ, Tijssen MP, Wildberger JE (2012) Dual-energy CT of the brain and intracranial vessels. AJR Am J Roentgenol 199:S26–S33

9. Schneider D, Apfaltrer P, Sudarski S et al (2014) Optimization of kiloelectron volt settings in cerebral and cervical dual-energy CT angiography determined with virtual monoenergetic imaging. Acad Radiol 21:431–436

10. Brockmann C, Scharf J, Nolte IS, Seiz M, Groden C, Brockmann MA (2010) Dual-energy CT after peri-interventional subarachnoid haemorrhage: a feasibility study. Clin Neuroradiol 20:231–235

11. Gupta R, Phan CM, Leidecker C et al (2010) Evaluation of dual-energy CT for differentiating intracerebral hemorrhage from iodinated contrast material staining. Radiology 257:205–211

12. Phan CM, Yoo AJ, Hirsch JA, Nogueira RG, Gupta R (2012) Differentiation of hemorrhage from iodinated contrast in different intracranial compartments using dual-energy head CT. AJNR Am J Neuroradiol 33:1088–1094

13. Tijssen MP, Hofman PA, Stadler AA et al (2014) The role of dual energy CT in differentiating between brain haemorrhage and contrast medium after mechanical revascularisation in acute ischaemic stroke. Eur Radiol 24:834–840

14. Watanabe Y, Tsukabe A, Kunitomi Y et al (2014) Dual-energy CT for detection of contrast enhancement or leakage within high-density haematomas in patients with intracranial haemorrhage. Neuroradiology 56:291–295

15. Ferda J, Novak M, Mirka H et al (2009) The assessment of intracranial bleeding with virtual unenhanced imaging by means of dual-energy CT angiography. Eur Radiol 19:2518–2522

16. Jiang XY, Zhang SH, Xie QZ et al (2015) Evaluation of virtual noncontrast images obtained from dual-energy CTA for diagnosing subarachnoid hemorrhage. AJNR Am J Neuroradiol 36:855–860

17. (2007) The 2007 Recommendations of the International Commission on Radiological Protection. ICRP publication 103. Ann ICRP 37:1–332

18. Toepker M, Moritz T, Krauss B et al (2012) Virtual non-contrast in second-generation, dual-energy computed tomography: reliability of attenuation values. Eur J Radiol 81:e398–e405

19. Kaufmann S, Sauter A, Spira D et al (2013) Tin-filter enhanced dual-energy-CT: image quality and accuracy of CT numbers in virtual noncontrast imaging. Acad Radiol 20:596–603

20. De Cecco CN, Darnell A, Macias N et al (2013) Virtual unenhanced images of the abdomen with second-generation dual-source dual-energy computed tomography: image quality and liver lesion detection. Investig Radiol 48:1–9

21. De Cecco CN, Buffa V, Fedeli S et al (2010) Dual energy CT (DECT) of the liver: conventional versus virtual unenhanced images. Eur Radiol 20:2870–2875

22. Graser A, Johnson TR, Hecht EM et al (2009) Dual-energy CT in patients suspected of having renal masses: can virtual nonenhanced images replace true nonenhanced images? Radiology 252:433–440

23. Sahni VA, Shinagare AB, Silverman SG (2013) Virtual unenhanced CT images acquired from dual-energy CT urography: accuracy of attenuation values and variation with contrast material phase. Clin Radiol 68:264–271